NUMERICAL SIMULATION OF THE TURBULENT HEAT TRANSFER IN A PIN-FINNED CHANNEL

João Felipe Mitre
PEQ/COPPE/UFRJ, Caixa Postal 68502, CEP 21941-972 – Ilha do Fundão, RJ
mitre@peq.coppe.ufrj.br
Ricardo Barbosa Damian
PEQ/COPPE/UFRJ, Caixa Postal 68502, CEP 21941-972 – Ilha do Fundão, RJ
ricardo@esss.com.br
Paulo Laranjeira da Cunha Lage
PEQ/COPPE/UFRJ, Caixa Postal 68502, CEP 21941-972 – Ilha do Fundão, RJ
paulo@peq.coppe.ufrj.br
Jian Su
PEN/COPPE/UFRJ, Caixa Postal 68509, CEP 21945-970 – Ilha do Fundão, RJ
sujian@con.ufrj.br

Abstract. *Fins are surface extensions designed to enhance heat transfer through the surface area increase. Pin fins heat exchangers use this principle in a compact manner. Their industrial applications are increasing, spanning from microprocessors to airplane turbines. This work investigates the turbulent heat transfer in a pin-finned channel using numerical simulation. Pins of cylindrical geometry using in-line and staggered arrangement were considered, in order to reproduce experimental data obtained from the literature. The main purpose of this work was to develop and validate a numerical model to the pin-finned channel flow to be used to evaluate other arrangements and flow conditions. The numerical simulations were carried out using a commercial CFD (Computational Fluid Dynamics) package, the CFX from ANSYS, and employed an advanced RANS (Reynolds Averaged Navier-Stokes) turbulence model, the SST (Shear Stress Transport). The numerical results for the global Nusselt number were shown to be in good agreement with available experimental data for several flow conditions.*

Keywords: *CFD, fin, pin-fin, heat exchangers, SST*

1. Introduction

Fins are surface extensions designed to enhance the heat exchange through the surface area increase. The heat transfer occurs by convection through the fins external area and by conduction inside the fins. Heat exchangers are widely used in industry in applications as air conditioning, motors cooling, electrical components cooling, and many others.

Aiming at maximizing the surface area for the convective heat transfer, pin fins heat exchangers are compounded by a large number of small pins. Another important point is that the close packing of pins inside the heat-exchanger channel produces high turbulence levels, enabling the design of efficient compact heat exchanger. This concept become suitable for applications where large amounts of heat need to be transferred and space limitation are mandatory in the design, as in microprocessors and airplane turbines cooling.

The heat transfer coefficients in a pin-finned channel are highly sensitive to the pin-fin geometry, pin arrangements along the channel and flow regime. There are some previous works that studied experimentally these parameters, and there are others that investigated numerically some simplified configurations. Bazdidi-Tehrani and Naderi-Abadi (2004) studied numerically the laminar fluid flow and heat transfer in the entrance region of a two dimensional horizontal channel with in-line fins. You and Chang (1997) studied the numerical prediction of heat transfer coefficient for turbulent flow for a pin-finned channel. Yuan (2000) carried out a numerical study of heat transfer in a channel with transverse fin arrays with periodic boundary conditions. Acharya and Saha (2003) solved numerically the turbulent transient flow around one rectangular pin-fin in laminar regime using periodic boundary conditions, showing the highly transient characteristic of the unstable flow around fins, even in laminar flows. Chyu *et al*. (1999) developed a mass transfer experiment enabling the evaluation of the heat transfer in pin-finned channels by analogy. Won *et al*. (2004) investigated the local Nusselt number calculated from experiments and discussed the unsteadiness of the flow in a channel with circular pin fins and its influence on heat transfer. They showed that the fluid flow in the pin-finned channel is essentially transient.

The present work numerically studied the fluid flow and heat transfer in a pin-finned channel. Differently from previous works, the whole pin-finned channel, and not only one fin with periodic boundary conditions, was simulated. Morevover, to the authors' knowledge, this was the first application of the SST (Shear Stress Transport) turbulence model to the heat transfer problem in pin-finned channels. Channels with cylindrical pins of constant cross section in aligned and staggered arrangements were considered. Our aim was to reproduce numerically the heat transfers coefficients experimentally determined which are available in the literature, developing, thus, an accurate numerical procedure that can be used to investigate other pins configurations.

2. Mathematical Modeling

We consider here three-dimensional, transient, turbulent flow of an incompressible Newtonian fluid with constant thermophysical properties. The continuity equation is given by:

$$\nabla \bullet \mathbf{U} = 0 \tag{1}$$

where ρ is the specific mass, **U** is the velocity vector and *t* is the time. The Reynolds averaged Navier-Stokes equations are given by:

$$\frac{\partial \rho \mathbf{U}}{\partial t} + \nabla \bullet (\rho \mathbf{U} \otimes \mathbf{U}) - \nabla \bullet (\mu_{eff} \nabla \mathbf{U}) = \nabla p' + \nabla \bullet (\mu_{eff} \nabla \mathbf{U})^T + \mathbf{B} \tag{2}$$

where **B** is the body force vector, null on this study, μ_{eff} is the effective viscosity and *p'* is turbulent modified pressure which are defined by:

$$p' = p + \frac{2}{3}\rho k \tag{3}$$

$$\mu_{eff} = \mu + \mu_t \tag{4}$$

where *p* is pressure, *k* is the kinetic turbulence energy, μ_t is the turbulent viscosity (see at equation 10), μ is the fluid molecular viscosity and ς is the fluid bulk viscosity.

Finally, the Reynolds averaged energy equation is given by:

$$\rho c_p \frac{\partial T}{\partial t} + \rho c_p \nabla \bullet \left[\mathbf{U} T \right] = \nabla \bullet \left(\left(\lambda + \frac{c_p \mu_t}{\mathrm{Pr}_t} \right) \nabla T \right) + S_E \tag{5}$$

where *T* is the temperature, c_p is the specific heat, λ is the thermal conductivity, Pr_t is the turbulent Prandt number, assumed to be 0.9, and S_E is the thermal source term, null in this study.

The turbulence model chosen for this work was the SST – *Shear Stress Transport* (Menter *et al*., 2002), which is specially indicated for calculation of skin friction and heat flux at solid surface. This model is a blend of the *k*-ω and *k*-ε turbulence models, near and far from the wall, respectively, where each of them gives better results.

The transformed equations for the *k*-ε and the Wilcox *k*-ω turbulence models (used in the SST model, Menter *et al*., 2002) are:

$$\frac{\partial (\rho k)}{\partial t} + \nabla \bullet (\rho \mathbf{U} k) = \nabla \bullet \left[\left(\mu + \mu_t \sigma_k \right) \nabla k \right] + \widetilde{P}_k - \beta^* \rho \omega k \tag{6}$$

$$\frac{\partial \left(\rho \omega \right)}{\partial t} + \nabla \bullet \left[\rho \mathbf{U} \omega \right] = \nabla \bullet \left[\left(\mu + \mu_t \sigma_\omega \right) \nabla \omega \right] + 2 \left(1 - F_1 \right) \rho \sigma_{\omega 2} \frac{1}{\omega} \nabla k \bullet \nabla \omega + \frac{\alpha}{\nu_t} P_k - \beta \rho \omega^2 \tag{7}$$

where ω is the turbulence frequency and $\nu_t = \mu_t / \rho$. P_k is the shear production of turbulence and its limiter are defined by:

$$P_k = \boldsymbol{\tau} : \nabla \mathbf{U} \quad \rightarrow \quad \widetilde{P}_k = \min(P_k, 10 \beta^* \rho k \omega) \tag{8}$$

where the Reynolds stress tensor is given by $\boldsymbol{\tau} = 2\mu_t \mathbf{D} - \frac{2}{3}\rho k \boldsymbol{\delta}$, where $\mathbf{D} = \frac{1}{2}\left[\nabla \mathbf{U} + \left[\nabla \mathbf{U} \right]^T \right]$.

All model constants are computed by blending the corresponding constants of the *k*-ε and the *k*-ω model using a blending function F_1 by $\alpha = \alpha_1 F_1 + \alpha_2 (1 - F_1)$, where α_1 and α_2 stands for the *k*-ω and the *k*-ε model constants, respectively. The constants for these models are: β^*=0.09, α_1=5/9, β_1=3/40, σ_{k1}=0.85, $\sigma_{\omega 1}$=0.5, α_2=0.44, β_2=0.0828, σ_{k2}=1, $\sigma_{\omega 2}$=0.856.

The first blending function F_1 is defined as:

$$F_1 = \tanh\left\{\left\{\min\left[\max\left(\frac{\sqrt{k}}{\beta^*\omega y}, \frac{500\nu}{y^2\omega}\right), \frac{4\rho\sigma_{\omega 2}k}{CD_{k\omega}y^2}\right]\right\}^4\right\} \tag{9}$$

where $CD_{k\omega}$ is

$$CD_{kw} = \max\left(2\rho\sigma_{\omega 2}\frac{1}{\omega}\nabla k \bullet \nabla\omega, 10^{-10}\right) \tag{10}$$

and y is the distance to the nearest wall.

F_1 is equal to zero away from the surface (k-ε model), and switches to one inside the boundary layer (k-ω model). The turbulent eddy viscosity is defined as follows:

$$\nu_t = \frac{a_1 k}{\max\left(a_1\omega, SF_2\right)} \tag{11}$$

where $a_1 = 0.31$, S is the invariant measure of the strain rate given by $\sqrt{2\,\mathbf{D}:\mathbf{D}}$ and F_2 is a second blending function defined by:

$$F_2 = \tanh\left[\left[\max\left(\frac{2\sqrt{k}}{\beta^*\omega y}, \frac{500\nu}{y^2\omega}\right)\right]^2\right] \tag{12}$$

This model requires the knowledge of the distance between the nodes and the nearest wall for performing the blending between the k-ε and k-ω models. The wall scale equation is solved to get these wall distances:

$$\nabla^2\phi = -1 \tag{13}$$

where ϕ is the value of the wall scale. The wall distance (WD) can be calculated from the wall scale through:

$$WD = \sqrt{\left|\nabla\phi\right|^2 + 2\phi} - \left|\nabla\phi\right| \tag{14}$$

The mathematical model given by Eqs. (1-14) is solved numerically by using the commercial CFD package *ANSYS CFX-5.7* (ANSYS, 2003). The CFX-5.7 code uses the Element Based Finite Volume Method – EBFVM, which allows the solution of mixed unstructured grids with the conservative nature of the Finite Volume Method (Maliska, 2004). This code carries out the numerical solution of the discretized momentum and mass balance equations using a fully implicit coupled solver with a multigrid strategy.

The results presented here came from simulations that employed the *High Resolution* advection scheme, which consists in a locally computed blend factor between first and second order UDS (Upwind Differencing Scheme) depending on flow conditions.

3. Experimental Validation

The validation of the numerical simulations was based on the experimental work of Chyu *et al.* (1999). This work studied the heat transfer in arrays with cylindrical pin-fins using in line and staggered arrangement.

Chyu *et al*. (1999) developed an experiment of mass transfer and study heat transfer by analogy. On this experiment, dry air was blown inside the finned channel compounded by pins made of aluminum with a thick layer of naphthalene on the surface. The naphthalene layer present only in the pin surface were obtained immersing the pins in a liquid bath of naphthalene during approximately one second, forming a homogeneous layer of about 0.5 mm thickness.

Measuring the total mass of naphthalene before the experiment and after 30 minutes of run, the mean mass transfer coefficient was calculated for a given configuration. By heat transfer analogy, the mean heat transfer coefficient was

also calculated. The experiment was carried out with constant temperature and, therefore, fluid properties remained constant too.

During the experiment, the system temperature was assumed to be the average temperature measured by four thermocouples sensors embedded in the inner surface of the two channel finned walls. Experimental results were discarded if the temperature measurements differed by more than 0.2 °C. Such a strict control of the temperature was necessary for determining the correct naphthalene vapor concentration on the fin surface. The average sublimed masses of naphthalene during the experiments were around 30 mg, weighed using an electronic balance with an accuracy of 0.01 mg for a sample of 166 g.

The pin-fin channel geometrical configurations used in these experiments area given in Figures 1. These figures show that the fins were disposed in the channel in 7 rows of 5 or 4 fins for inline and staggered arrangements, respectively. The relevant dimensions of these configurations are D = 12.5 mm and S = X = 2.5 D. The length of the pin fins is equal to D. The channel had a rectangular cross section 159 mm wide and with height equal to D. In the experiment, a long initial unfinned section was used to stabilize and develop the flow.

In our simulations, the fluid was assumed air with constant properties at 25°C and 1 atm for better correlation with experimental conditions.

4. Computational Domain, Grid and Boundary Conditions

The 3D computational domain included a 40 mm long section before the first line of pins (upstream) and an 80 mm section after the last line of pins (downstream), resulting in an overall channel length of 320 mm. The channel hydraulic diameter (D_h) is 23.5 mm and it was used to evaluate the Reynolds number:

$$\mathrm{Re}_D = \frac{\rho U_\infty D_h}{\mu} \tag{15}$$

where U_∞ is an average velocity of gas on inlet.

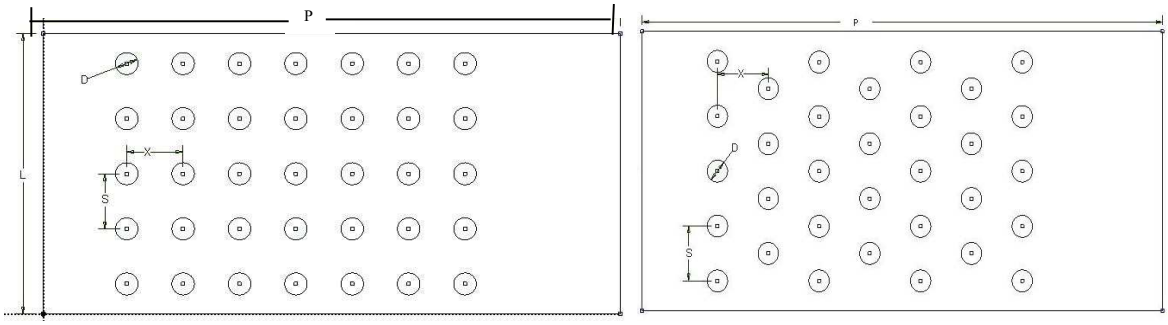

(a) (b)

Figure 1: Pin-fin channel: (a) inline and (b) staggered arrays.

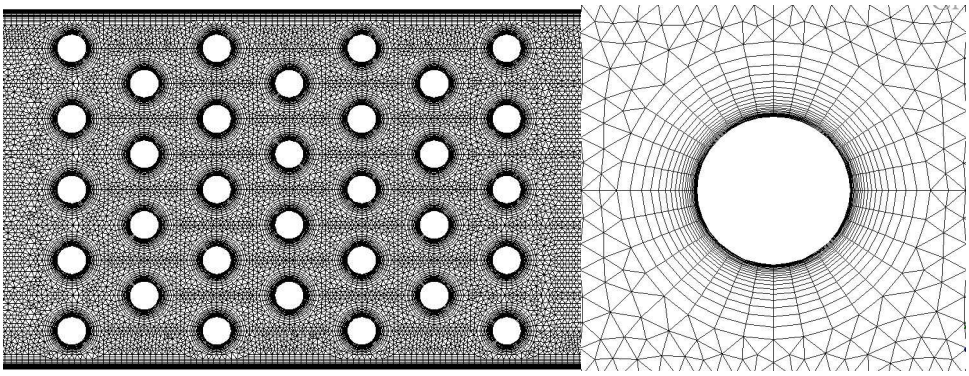

Figure 2: Mesh cut view and near fin mesh refinement.

The domain discretization was carried out using hybrids meshes compounded by prismatic and hexahedral elements. The mesh was extruded in the channel height direction with 30 elements symmetrically refined near the upper and lower channel walls with a growth rate of 1.3. The global size of the mesh was 3 mm. The cylindrical fin surface had

element for each 10 degrees (about 1.1 mm). Near the fin walls, it was employed a normal mesh extrusion consisting of 23 layers whose thickness grew at a factor of 1.2 away from the surface. The first extrusion layer height was 0.02 mm. In general, the meshes had about 1.200.000 nodes (Figure 2).

This wall refinement for the fins results in an *Element Aspect Ratio* about 55 and a maximum value of y^+ (the dimensionless distance from the nearest wall, given by $y^+ = \rho y \sqrt{\tau_\omega / \rho} / \mu$, where τ_ω is the wall shear stress) of about 3.6, which was calculated by post-processing the simulation results. These values are considered well suitable for an accurate near wall calculation with the SST model.

In the channel inlet, it was prescribed a constant velocity profile (as a function of the prescribed Re_D, according to the experimental runs) and temperature of 25 °C. The channel walls were considered adiabatic and the fins walls had a constant prescribed temperature of 30°C. No-slip boundary conditions (null velocity components) were assumed at all solid boundaries. At the channel outlet, the boundary condition called *Opening* by the CFX code was used. It consists of the prescription of a mean average relative static pressure (in this case, zero) with the possibility of reflux. This boundary condition allows the usage of short downstream domains, which reduces the mesh size. In case of reflux, the inflow fluid temperature was set to be the mean outlet temperature.

5. Results and Discussions

The simulations required about 2.3 GiB of RAM memory and they were executed in parallel (using the MPICH parallelization library) with 2 or 3 Pentium IV processors at 3 GHz. CFX steady-state simulation with the same uniform time steps for all variables were employed. These are effectively transient simulations with coefficient lagging. In general, using the residual criteria (RMS value of the normalized residuum of all flow variables at each mesh node) of 10^{-4}, the convergence was reached in approximately 250-750 iterations. The simulations took about 3-7 hours in this cluster.

The Nusselt number was calculated by:

$$Nu = \frac{hD_h}{\lambda} = \frac{\left(\frac{q}{A\Delta T}\right)D_h}{\lambda} \tag{16}$$

where h is the heat transfer coefficient, A is the area of all pins, λ is the thermal conductivity and q is the total heat transfer rate. The temperature difference, ΔT, was defined to be 5 °C in the simulations, as described above. The heat transfer rate, q, was evaluated by post-processing the simulation results.

All results for the Nusselt number were in good agreement with the experimental data, as can be seen in Figure 3. The larger relative deviation in Nusselt number was approximately 4%, which occurred for the highest Reynolds number simulation with the staggered arrangement.

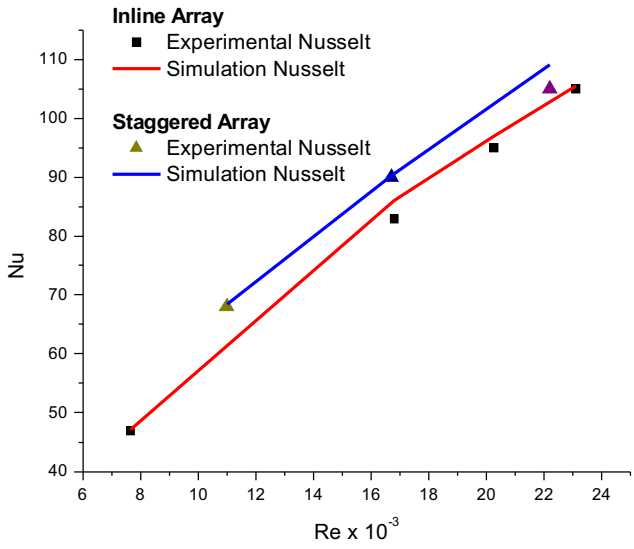

Figure 3: Comparison between the experimental and simulated Nusselt number data.

For all Reynolds number values, the highest turbulence level and mixing intensity were always observed in the staggered configuration. The results shown in Figure 3 confirmed that the staggered configuration leads to a higher heat transfer coefficient when compared to the inline configuration.

Some difficulties were faced in carrying out these simulations. The principal difficulty was the unstable character of the flow around the cylinders. The flow instability generated in one cylinder is propagated to the next cylinder array and so on, increasing in magnitude. This kind of behavior clearly characterizes transient flow. Since the magnitude of these flow instabilities were sufficiently small, solutions obtained through the CFX steady-state simulation could achieve the not too strict convergence criterion used. Although a CFX transient simulation would give a better representation of the transient flow in these pin-fin channels, the CFX steady state simulation sufficed for Nusselt number evaluation, saving a lot of computational time. A careful mesh construction has shown to be an important factor in reducing the convergence difficulties in the simulations. Several meshes morphologies and refinements were tested and two conclusions could be made: (i) too much mesh refinement made the convergence of the steady state more difficult, probably because the increasing capability of capturing flow instabilities of small vortexes; (ii) the usage of mesh extrusion (normal to the pins walls), using a adequate element grown ratio (in length and volume), resulted in a mesh that could describe better the flow in the more interesting regions.

Figures 4 to 11 shown results for the simulations using Reynolds number values of 16,700 for the in-line array and 16,800 for the staggered array. It is possible to observe in Figure 4 that there is no symmetry in the velocity contours, which is a consequence of the transient characteristic of these flows. This behavior is also shown in the Fig. 5, which presents the heat transfer rates for some fins along a few solver iterations. For a true steady state solution, all the heat rate values would be constant. Figure 5 clearly shows that there are small oscillations in the heat transfer rate for each fin. On the other hand, as shown in Figure 6, the total heat transfer rate (in all fins) is clearly more stable along the solution iterations. This is a consequence to the fact that the quasi-periodic oscillations of heat transfer rates for the fins are not in phase, therefore, the overall heat transfer rate oscillates with a much smaller amplitude. It should be pointed out that only a few iterations were shown in Figures 5 and 6 for better visualization.

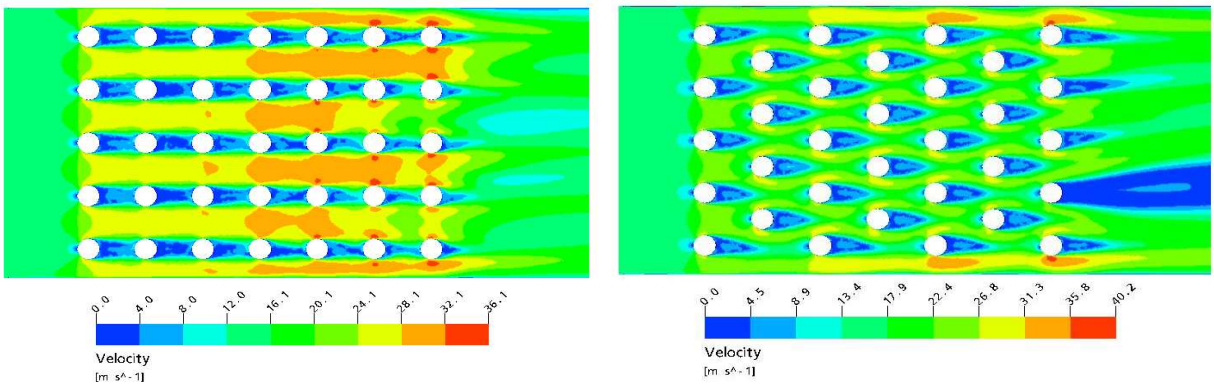

(a) (b)

Figure 4: Velocity contours: (a) inline and (b) staggered arrays.

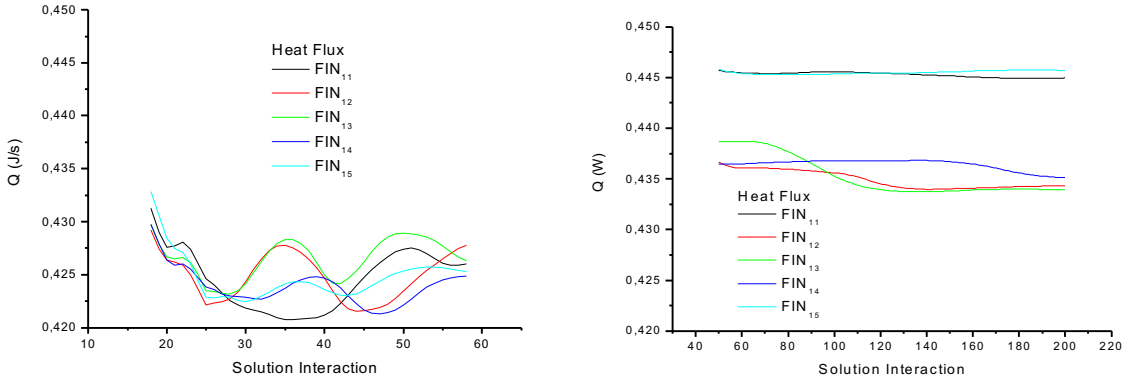

(a) (b)

Figure 5: Heat flux in the fins: (a) inline and (b) staggered arrays. The matrix index FIN_{ij} represents the fin at line *i* and column *j*.

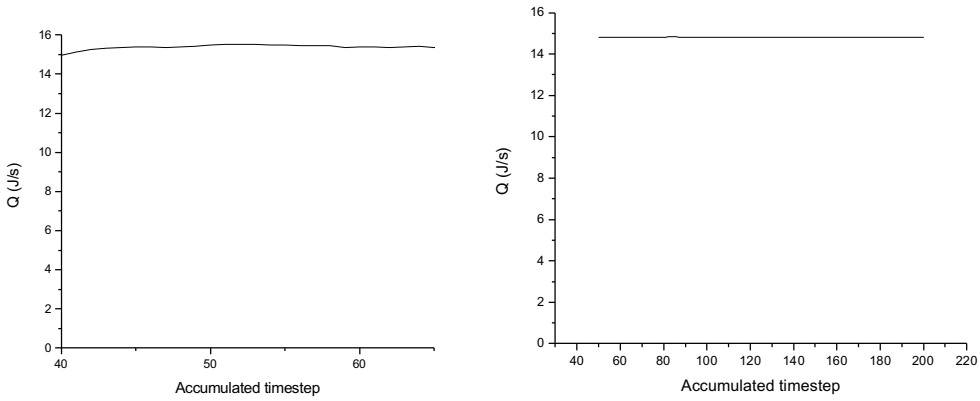

(a) (b)

Figure 6: Total heat flux in all fins: (a) inline and (b) staggered arrays.

Figure 7 illustrates the streamlines near the fins colored accordingly to the velocity value. Vortex instabilities can be clearly observed in the in-line fin arrangement. The CFX steady-state simulation converged with the RMS residues below 10^{-4} for all variables and even so, the solution is still asymmetrical. Analyzing the instantaneous solutions for different iterations, it could be observed that these unstable vortexes were continuously changing position. Figure 8 shows the temperature contours, where there is also no symmetry. Figure 9 illustrate y^+ on the fin walls, whose values vary up to 3.6.

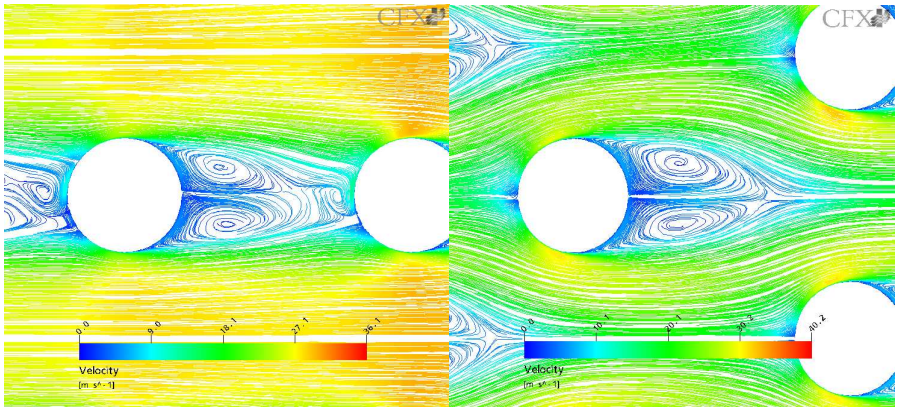

(a) (b)

Figure 7: Velocity streamlines: (a) inline and (b) staggered arrays.

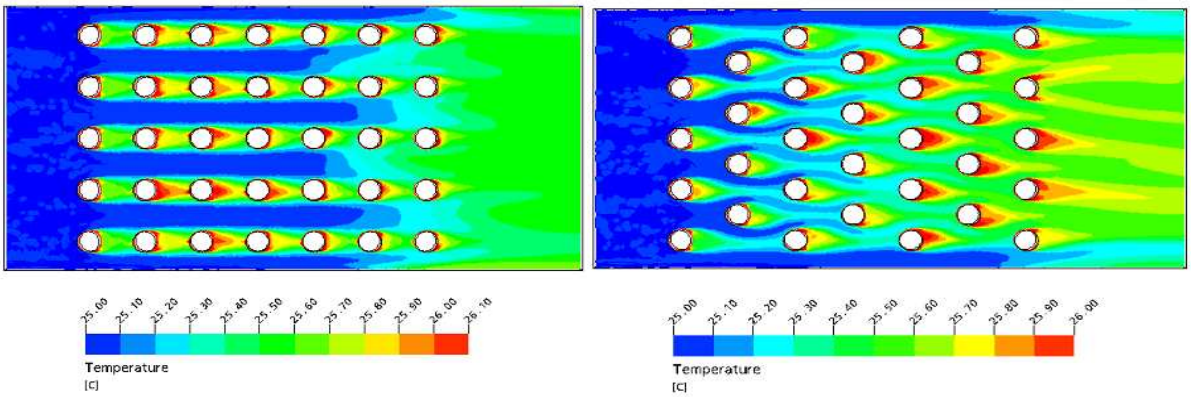

(a) (b)

Figure 8: Temperature contours (red color represent temperatures up to 30°C): (a) inline and (b) staggered arrays.

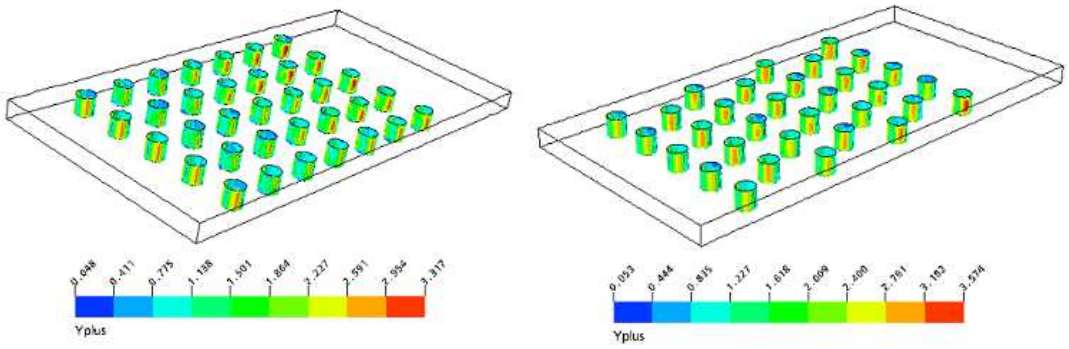

(a) (b)

Figure 9: y^+ contours on the fin surfaces: (a) inline and (b) staggered arrays.

6. Conclusions

Flows around bluff bodies (non-aerodynamic) are naturally transient due to an unstable vortex street behind them. If there is a quasi-periodic flow in which the amplitude of such oscillations are not too large, a transient simulation with coefficient lagging, as the CFX steady-state simulation, can rapidly reach a solution for this quasi-steady regime which represents its flow characteristic within a small error associated to the oscillation amplitude.

CFX steady-state simulations using the SST turbulence model were employed to evaluate the heat transfer in pin-finned channels with inline and staggered configurations. For the conditions analyzed in this work, the flows through the pin-finned channels reached quasi-periodic regimes. The total heat transfer rates were evaluated, whose values oscillated much lesser than the fin heat transfer rates due to out of phase behavior of the latter. Therefore, the global Nusselt numbers could be evaluated with good accuracy from the CFX steady-state simulations and their values compared favorably to the available experimental data.

Although transient simulations should be used to investigate deeper the velocity and temperature fields, the performance of the SST turbulence model in predicting the global heat transfer rate can be regarded as very good.

7. Acknowledgements

The authors acknowledge FAPERJ and CNPq (grant no. 351378/1994-4) by the financial support during the realization of this work

8. References

Acharya, S., Saha, A. K., 2003, “Parametric Study of unsteady flow and heat transfer in a pin-fin heat exchanger”, International Journal of Heat and Mass Transfer, vol. 46 , pp. 3815-3830.

Bazdidi-Tehrani, F., Naderi-Abadi, M., 2004, “Numerical analysis of laminar heat transfer in entrance region of a horizontal channel with transverse fins”, International Comm. in Heat and Mass Transfer, vol. 31, pp. 211-220.

ANSYS, 2003, CFX-5.7 User Manual.

Chyu, M. K., Hsing, Y. C., Shih, T. I.P., Natarajan, V.; 1999, “Heat Transfer Contribuitions of Pins and Endwall in Pin-fin Arrays: Effects of Thermal Boundary Condition Modeling”, Journal of Turbomachinery, vol. 121, pp. 257-263.

Maliska, C., 2004, "Transferência de Calor e Mecânica dos Fluidos Computacional", 2a Edição, LTC.

Menter, F., Vieser, W., Esch, T., 2002,“Heat Transfer Predictions using Advanced Two-Equation Turbulence Models”, CFX-Validation Report, CFX-VAL10/0602.

Won, S. Y., Mahmood, G. I., Ligrani, P. M., 2004, “Spatially-resolved heat transfer and flow structure in a rectangular channel with pin fins”, International Journal of Heat and Mass Transfer, vol. 47, pp. 1731–1743.

You, H. I., Chang, C. H., 1997, “Numerical prediction of heat transfer coefficient for a pin-fin channel flow”, Journal of Heat Transfer-Transactions of the ASME, vol. 119, pp. 840-843.

Yuang, Z. X., Chang, C. H., 2000, “Numerical study of periodically turbulent flow and heat transfer in a channel with transverse fin arrays”, International Journal of Numerical Methods for Heat & Fluid Flow, vol. 10, pp. 842-861.